Investigation of Microphysical Processes Occurring in Organized Convection during NAME

ANGELA K. ROWE, STEVEN A. RUTLEDGE, AND TIMOTHY J. LANG

Department of Atmospheric Science, Colorado State University, Fort Collins, Colorado

(Manuscript received 3 May 2011, in final form 6 February 2012)

ABSTRACT

A major objective of the North American Monsoon Experiment (NAME) was to quantify microphysical processes within convection occurring near the steep topography of northwestern Mexico. A previous study compared examples of isolated convection using polarimetric radar data and noted a dependence on mixed-phase processes via drop freezing and subsequent riming growth along the coastal plain and western slopes, with an even greater role of melting ice in rainfall production over the highest terrain. Despite the higher frequency of these isolated cells compared to organized convective systems, the latter were responsible for 75% of rainfall. Therefore, this study seeks to evaluate the role of mesoscale organization on microphysical processes and describes the evolution of these systems as a function of topography.

Similar to isolated convection, both warm-rain and ice-based processes played important roles in producing intense rainfall in organized convection. Although similarities existed between cell types, organized convection was typically deeper and contained greater ice mass, which melted and contributed to the development of outflow boundaries. As convection organized along the slopes, these boundaries spread over the lower terrain, converging with diurnally driven upslope flow, thus allowing for the generation of new convection and propagation toward the coast. Once over lower elevations, additional warm-cloud depth contributed to intense rainfall and allowed for continued ice production. This, along with the development of rear inflow in the trailing stratiform region, led to further development of convective outflow, similar to organized systems in the tropics and midlatitudes.

1. Background and motivation

The arrival of strong convection in the semiarid regions of the southwestern United States and northwestern Mexico during mid to late June marks the onset of the North American monsoon (NAM). This atmospheric circulation develops as a result of land–sea temperature contrast, and similar to its Asian counterpart, is characterized by a reversal of the mean low-level winds, which ushers moist flow from the Gulf of California onshore into northwestern Mexico. Within a horizontal distance of less than 200 km, the warm waters of the gulf transition to the steep topography of the Sierra Madre Occidental (SMO), extending more than 3 km above sea level. It is well known that diurnally forced land–sea and mountain–valley flows affect the timing and distribution of precipitation in this region (Douglas et al. 1993; Dai et al. 1999). More specifically, results from the North American Monsoon Experiment (NAME; Higgins et al. 2006) found a strong topographical influence on the diurnal variability of rainfall (e.g., Gochis et al. 2004, 2007; Lang et al. 2007), where frequent afternoon convection occurred over the SMO, dissipating by early evening. Under certain conditions, this convection grew upscale to form larger, organized, mesoscale convective systems (MCSs) that propagated toward the gulf. This promoted a less frequent but more intense late-evening/early-morning peak in precipitation across lower elevations (Lang et al. 2007). In addition to this coast-perpendicular movement of organized systems (defined as regime A by Lang et al. 2007), periods when phase velocities were characterized by northward along-coast propagation were also identified (regime B, same study). These systems were characterized by longer lifetimes and persisted well into the early morning hours over the gulf. On occasion, MCSs displayed both along- and cross-coast movement,

Corresponding author address: Angela K. Rowe, Department of Atmospheric Science, Colorado State University, Fort Collins, CO 80523.
E-mail: arowe@atmos.colostate.edu

DOI: 10.1175/MWR-D-11-00124.1

leading to a combined classification referred to as regime AB by Lang et al. (2007).

The processes by which convection initiates and organizes once off the SMO need to be better understood to properly represent the diurnal cycle of precipitation in numerical models. In addition, the evolution of microphysical processes must be studied to provide a physical basis for estimating precipitation via remote sensing (e.g., Nesbitt et al. 2008). Hydrometeor identification using polarimetric radar data provides a means to validate and improve microphysical and convective parameterizations, which are known to significantly affect numerical model simulations of the regional climate during the NAM (e.g., Gochis et al. 2002). Previous satellite- and radar-based studies of precipitating systems in this region have shown that convection over the SMO tends to be shallower than over the lower elevations and coastal plain (e.g., Nesbitt et al. 2008; Rowe et al. 2008). Nesbitt et al. (2008) also described a corresponding reduction in depth of precipitation-sized ice in convection over the high terrain, suggesting a greater dependence on warm-rain processes. However, Rowe et al. (2008) found that warm-cloud depths increased toward lower elevations, suggesting an increased role of coalescence growth in explaining the larger precipitation intensities over the lower terrain. In addition, the presence of graupel up to 10 km (MSL; assumed for all heights hereafter) in convection over the coastal plain was noted using profiler data (Lerach et al. 2010), suggesting an important contribution from ice-based processes over lower elevations as well.

Using three-dimensional gridded data from the National Center for Atmospheric Research S-band, polarimetric radar (S-Pol), Lang et al. (2010) found increased ice and water mass, greater rainfall intensity, and larger median drop sizes over the coastal plain relative to the high terrain. Furthermore, Rowe et al. (2011) selected NAME S-Pol volume scans with improved temporal and spatial resolution to investigate the evolution of microphysical characteristics associated with isolated convection over land. Increased water mass and rainwater depth were associated with convection over the lower elevations, consistent with the Lang et al. (2010) study, confirming the important role of warm-rain processes (Rowe et al. 2008).

A selection of cases over the lower elevations illustrated a clear dependence on mixed-phase processes, in addition to coalescence, via drop freezing and subsequent riming growth. In comparison, several examples of convection over the SMO revealed shallower coalescence zones and reduced graupel depth, consistent with previous studies (e.g., Nesbitt et al. 2008); however, the potential for higher elevations to receive brief periods of intense rainfall was also noted in these cases, as well as in previous general studies of NAME precipitation (e.g., Gochis et al. 2007; Rowe et al. 2008). Peak ice mass, occurring just above the melting level for all elevation groups, was greatest over the SMO, likely due to the shallower warm-cloud depth in cells over these higher elevations. Shallow warm-cloud depths limit coalescence, allowing for a greater percentage of condensate to be lofted above the freezing level, which ultimately leads to increased ice mass via riming and (occasional) intense rainfall over the higher terrain as these large ice hydrometeors melt. Indeed, a particularly deep cell over the SMO was characterized by rain rates >80 mm h^{-1}, despite the truncated warm-cloud depth.

Lang et al. (2007, 2010) noted increased rainfall during disturbed regimes (i.e., regimes A, B, and AB), as well as microphysical differences compared to nondisturbed times. More specifically, during regime AB, a greater increase in liquid water mass compared to ice mass was observed over the gulf (Lang et al. 2010), implying an increasingly important role of warm-rain processes compared to the nondisturbed periods (for isolated convection). A more modest change, however, was observed over the high terrain during these disturbed periods. To further investigate this suggested topographical dependence on microphysical processes associated with *organized* convection, this study focuses on the evolution of *individual* MCSs through a case study approach, using data from the S-Pol radar to describe hydrometeor characteristics as a function of terrain. In addition, cells associated with organized systems will be compared to isolated convective cells to better understand the proposed relationship between microphysical processes and organization.

2. Methods

During the NAME field campaign, the S-Pol radar, situated approximately 90 km north of Mazatlan along the gulf coast (see Fig. 1 of Rowe et al. 2008), provided nearly continuous data from 8 July through 21 August 2004. Low-level, 360° scans to a range of 250 km were completed every 15 min to map rainfall. A sector-scanning mode, with azimuthal widths ranging from 90° to 120° and maximum range of 150 km, was employed for about 95 h of scanning time for improved temporal and spatial resolution. Similar to the isolated cases in Rowe et al. (2011), examples of organized systems for this study were selected from these so-called microphysical scans, which allowed for improved temporal resolution and investigation of the evolution of the finescale vertical structure of embedded convection.

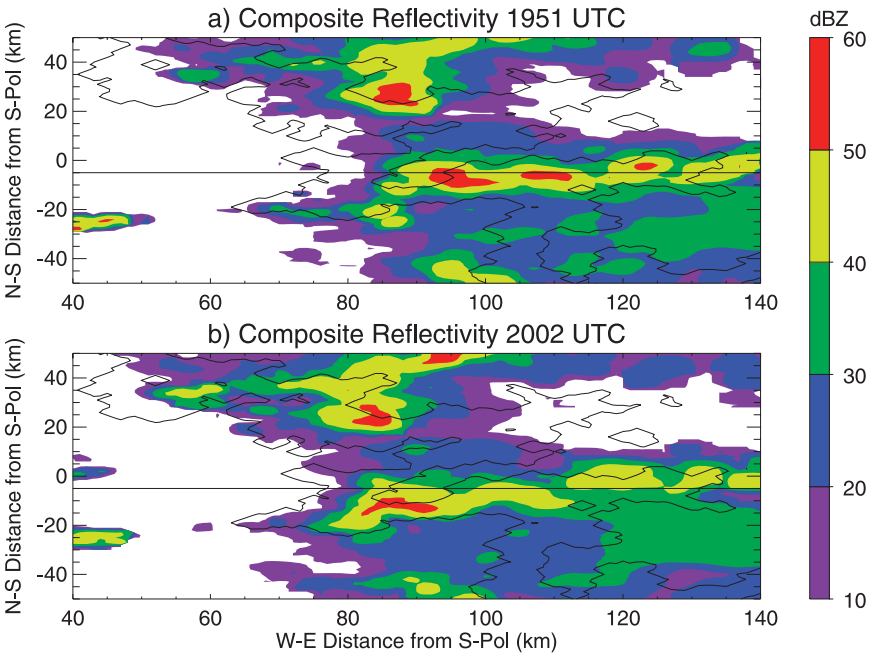

FIG. 1. Gridded composite reflectivity for (a) 1951 and (b) 2002 UTC 5 Aug 2004. Overlaid is terrain height, contoured from 0 to 3 km in 1-km increments. The black lines indicate the locations of the cross sections shown in Fig. 2.

Quality control of the S-Pol data is described in detail in previous NAME studies (e.g., Lang et al. 2007, 2009). Radar variables used in this study included radar reflectivity factor at horizontal polarization Z_H; differential reflectivity Z_{DR}; providing information about oblateness, linear depolarization ratio L_{DR}, and zero-lag cross-correlation coefficient $\rho_{HV}(0)$, both of which allow for discrimination between pure rain and mixtures of rain and ice; as well as specific differential phase K_{DP}, which depends on particle concentration, size, and shape and is correlated to liquid water content. More complete descriptions of these polarimetric variables can be found in Doviak and Zrnić (1993), Zrnić and Ryzhkov (1999), Bringi and Chandrasekar (2001), and Ryzhkov et al. (2005). Quality-controlled S-Pol data were then interpolated to a 1-km horizontal- and 0.5-km vertical-resolution Cartesian grid using REORDER (Mohr et al. 1986). The gridded polarimetric variables, along with a mean temperature profile (from the Mazatlan sounding), were then incorporated into a hydrometeor classification (HID) algorithm, based on the method of Liu and Chandrasekar (2000) and described by Tessendorf et al. (2005), to determine the dominant hydrometeor type at each grid point.

The gridded S-Pol dataset was then subjected to a cell identification and tracking algorithm, described in detail by Rowe et al. (2011). In general, cells were identified using an ellipse-fitting method (Nesbitt et al. 2006), based on reflectivity and area thresholds, providing a means to objectively classify convective elements. Specifically, reflectivity thresholds of 35 and 45 dBZ were applied to improve identification of intense convective echo embedded within larger features. To focus solely on MCSs, the locations of tracked cells were matched to precipitating features identified by Pereira (2008). Pereira used a feature identification algorithm, developed by Rickenbach and Rutledge (1998) and described by Lang et al. (2007) in the context of the NAME dataset, to classify feature types based on the following criteria: if the major axis of the feature exceeded 100 km, it was considered an MCS; furthermore, if the ratio between the major and minor axes of the convective area of the feature was more than five (following Bluestein and Jain 1985), the feature was classified as linear. For this study, all cells embedded within features defined as MCS scale, whether linear or nonlinear, were included to describe the evolution of cells within organized systems. Furthermore, cells in MCS convection are compared to isolated cells.

In addition to the polarimetric variables, several cell properties were computed to aid in the description of storm evolution and provide a means for comparison with isolated convection. Echo-top heights were estimated using the maximum height of the 0-dBZ reflectivity contour. Maximum Z_{DR} for each cell was computed for grid points within the cell identified as

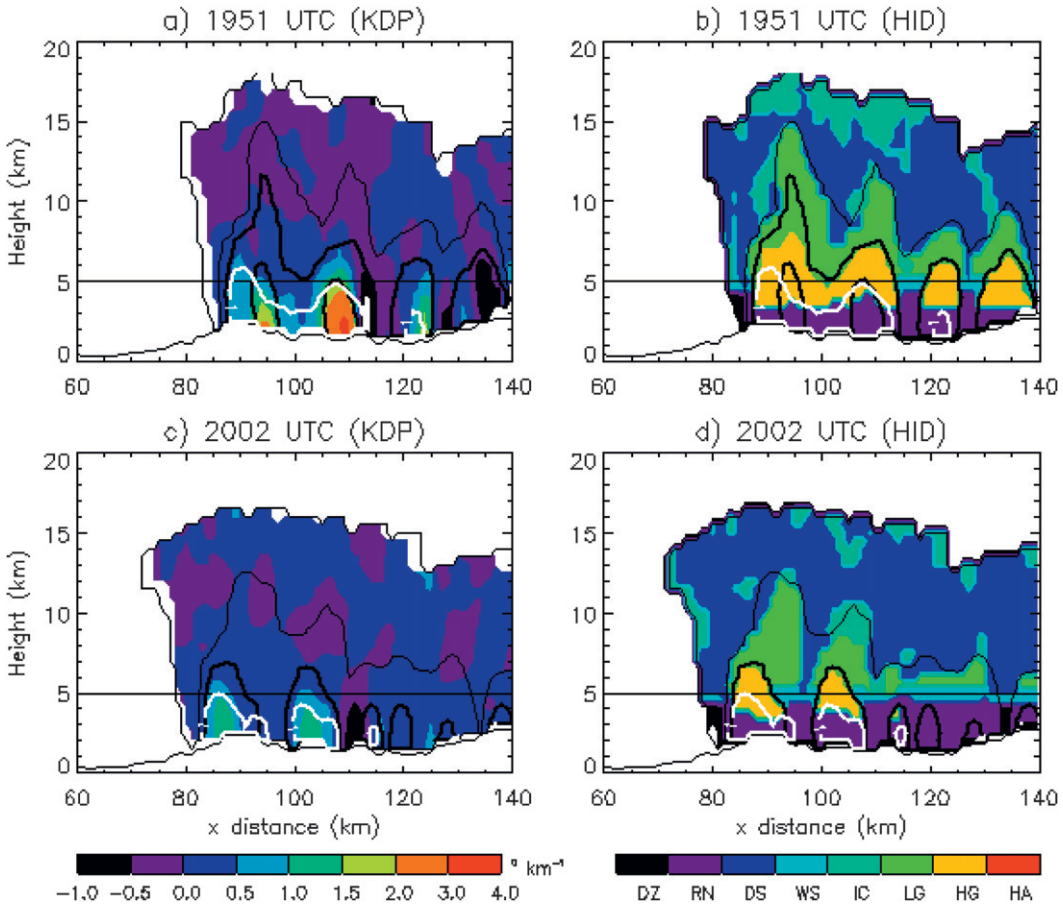

FIG. 2. Vertical cross sections through cells at (a),(b) 1951 and (c),(d) 2002 UTC 5 Aug 2004. Color-filled contours are associated with (left) K_{DP} (° km^{-1}) and (right) HID. The HID abbreviations correspond to the following classifications: drizzle (DZ), rain (RN), dry snow (DS), wet snow (WS), ice (IC), low-density graupel (LG), high-density graupel (HG), and hail (HA). Black contours represent reflectivity at 0, 30, 40, and 50 dBZ, with the 40- and 50-dBZ contours thickened. Values of Z_{DR} are contoured in white for 1 (solid) and 2 dB (dashed). Terrain height is plotted at the bottom as a black contour, and the solid black line at 5 km represents the average height of the melting level during NAME. The x axis is the distance from S-Pol in km.

rain by the HID and located below 4 km to reduce the effects of melting; the melting level was located, on average, at 5 km during NAME. Ice and liquid water masses were calculated using the same technique as the isolated cases (Rowe et al. 2011) and the Lang et al. (2010) study, following a methodology described by Carey and Rutledge (2000) and Cifelli et al. (2002). Ice (IWP) and liquid water (LWP) paths were computed by integrating ice and liquid water masses over the vertical columns associated with all grid points in individual convective cells. Ice and liquid water path ratios were then computed by dividing the IWP and LWP by the summation of the two, respectively.

Near-surface rain rates, calculated using polarimetric-based equations (Cifelli et al. 2002, 2011) that were used for previous NAME studies (e.g., Rowe et al. 2008, 2011), were also available for each cell, providing additional means for describing microphysical changes as these precipitating systems evolved. Although these particular rainfall relations were not necessarily shown to be the best choice for the region, they are adequate for describing relative differences. Nonuniform beam filling also potentially introduces errors in the rain-rate calculations, but only at large distances from the radar. Maximum terrain height was determined for each identified cell, using topographic data from the National Geophysical Data Center (NGDC). In addition to feature type, cells were grouped based on elevation using the same terrain thresholds used in previous NAME studies (Gochis et al. 2004; Rowe et al. 2008, 2011): 0–1 km, 1–2 km, >2 km, and over water. This allowed for comparisons of cell characteristics based on organization and topography. The following case studies will focus on MCSs that formed off the SMO, as well as

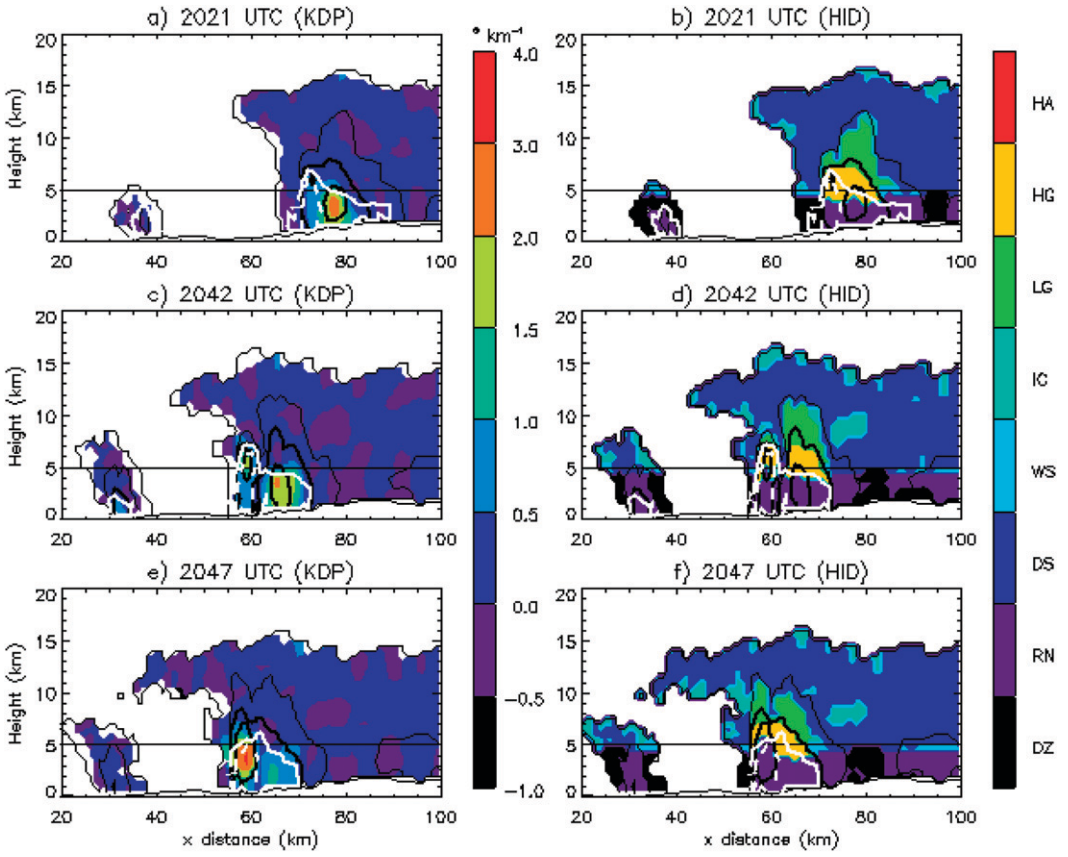

FIG. 3. Vertical cross sections through cells at (a),(b) 2021; (c),(d) 2042; and (e),(f) 2047 UTC 5 Aug 2004. See Fig. 2 for a description of the variables and contours.

those that moved into the domain, allowing not only for elevation-dependent trends over land to emerge, but to analyze differences between convection over land and water.

3. Case studies

a. 5–6 August

Under certain conditions, convection that initiated over the high terrain later organized and grew upscale while moving westward toward the coast. A representative example of this occurred during 5–6 August when a quasi-linear (i.e., classified as linear throughout some, but not all of its lifetime; different from the conventional definition of a quasi-linear convective system), asymmetric MCS developed along the SMO around 1800 UTC (5 August), propagated toward the radar, then moved toward the northwest after 2200 UTC, paralleling the coast and persisting past 0000 UTC (6 August). Because of this combined cross- and along-coast movement, this period was classified under regime AB (Lang et al. 2007). Environmental conditions were characterized by increased easterly zonal flow at mid- and upper levels due to an approaching upper-level jet streak, resulting in 0–6-km wind shear values reaching 8.5 m s^{-1} (Pereira 2008). In addition, an upper-level inverted trough to the southeast provided moisture advection into the domain during the afternoon of 5 August, leading to increased values of CAPE. Within this moist and sheared environment, the quasi-linear MCS developed during the evening hours.

The majority of convection during this time period was associated with organized systems over land, with 72% of cells classified as organized and only 2% of those over water. Around 1830 UTC, scattered convection developed over the SMO (>2 km) at the far eastern edge of the radar domain. By 1933 UTC, a west–east-oriented line of convection formed to the east of the radar, with additional convection developing to the east-northeast of the radar over the high terrain. At 1951 UTC, several cells to the east existed at various stages of their life cycles (Fig. 1a), with corresponding vertical cross sections (Figs. 2a,b) showing leading convection over a local maximum in the SMO terrain (at 90-km range) characterized by an echo-top height of 18 km,

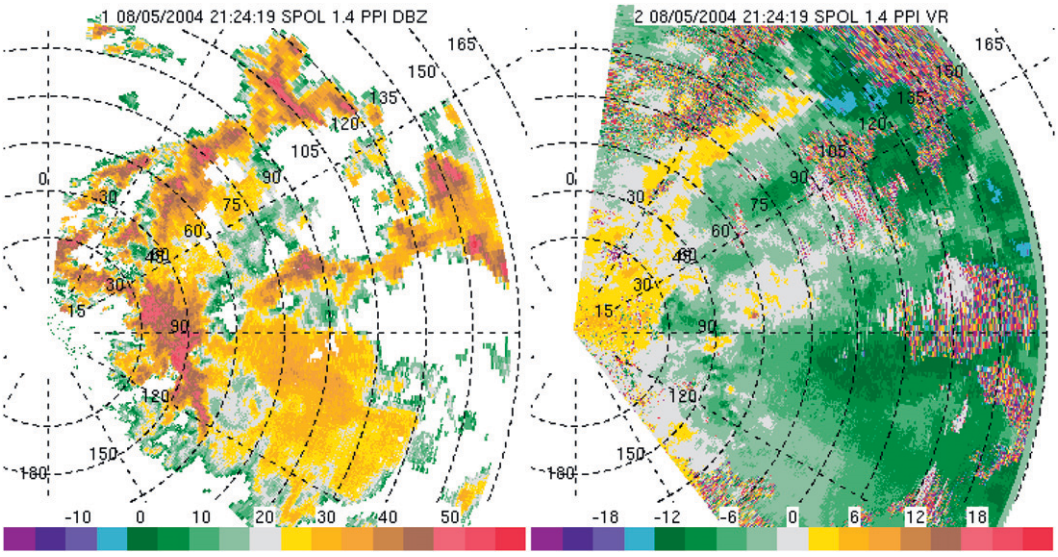

FIG. 4. PPI images of (left) reflectivity (dBZ) and (right) radial velocity (m s^{-1}) at 2124 UTC 5 Aug 2004 at 1.4°. Range rings are shown every 15 km and azimuths every 30°.

graupel extending to 15 km (Fig. 2b), and the 1-dB Z_{DR} contouring extending above 5 km, referred to as a Z_{DR} column. The presence of positive Z_{DR} above the melting level indicates the lofting of oblate raindrops into temperatures below 0°C (e.g., Hall et al. 1984; Illingworth et al. 1987), where they freeze and become embryos that promote rapid accretional growth leading to graupel. This characteristic was also observed in isolated convection over the coastal plain (Rowe et al. 2011) and has been noted for convection in a variety of locales (see references in Rowe et al. 2011). This cell was followed by a mature cell at 110 km with maximum K_{DP} values extending to the surface (Fig. 2a) and a shallower extent of graupel (Fig. 2b), indicating that precipitation was falling out. Even weaker cells were situated farther back over the terrain, although at these ranges, it was difficult to assess the storm's true intensity. Shortly after, at 2002 UTC (Fig. 1b), the cell at 110 km had weakened, characterized by reduced K_{DP} values near the surface (Fig. 2c) and a slightly shallower depth of graupel (Fig. 2d), with less continuity between cells compared to the previous time. The cells beyond 120 km had decayed, becoming an extensive trailing stratiform region, leaving a quasi-linear convective system along the western slopes. The collapse of convective cells to form stratiform precipitation areas is a common characteristic of MCSs in the midlatitudes (Houze 1993, 1997).

A vertical cross section through the leading convection to the east-southeast along the slopes at 2021 UTC (Figs. 3a,b) highlights a deep system, with echo tops exceeding 15 km and a Z_{DR} column evident at the leading edge. An elevated maximum in K_{DP} (Fig. 3a) beneath HID-identified high-density graupel (Fig. 3b) indicated the melting of ice hydrometeors, which appeared to be an important contributor to rainfall along the western slopes. Also at this time, new convection initiated ahead of the system between the 30- and 40-km range over the lower elevations as low-level onshore flow began to lift along slightly elevated terrain. In this developing convection, the majority of echo existed below the melting level, implying the importance of warm-rain processes early on. At 2042 UTC (Figs. 3c,d), a Z_{DR} column was again observed along the leading edge, with values ≥2 dB above the melting level, indicating lofting of large (oblate), liquid hydrometeors into the mixed-phase zone, contributing to a new area of HID-identified high-density graupel along the leading edge at 60 km (Fig. 3d). Values of K_{DP} remained large (>2° km^{-1}; Fig. 3c), indicating the continued melting of precipitation-sized ice above the slopes. The cell ahead of this system deepened, yet remained dominated by collision–coalescence due to the large warm-cloud depth and lack of HID-identified graupel. By 2047 UTC (Figs. 3e,f), the Z_{DR} column was no longer present, but a new maximum in K_{DP} of 3°–4° km^{-1} was observed along the leading edge, consistent with the melting (and fallout) of graupel and hail that were produced by frozen drops and subsequent riming. The previous K_{DP} maximum descended to near the surface at this time, further highlighting the multicellular nature of these systems.

A reflectivity PPI image from later at 2124 UTC (Fig. 4) reveals a nearly continuous leading line of convection moving off the western slopes. The corresponding

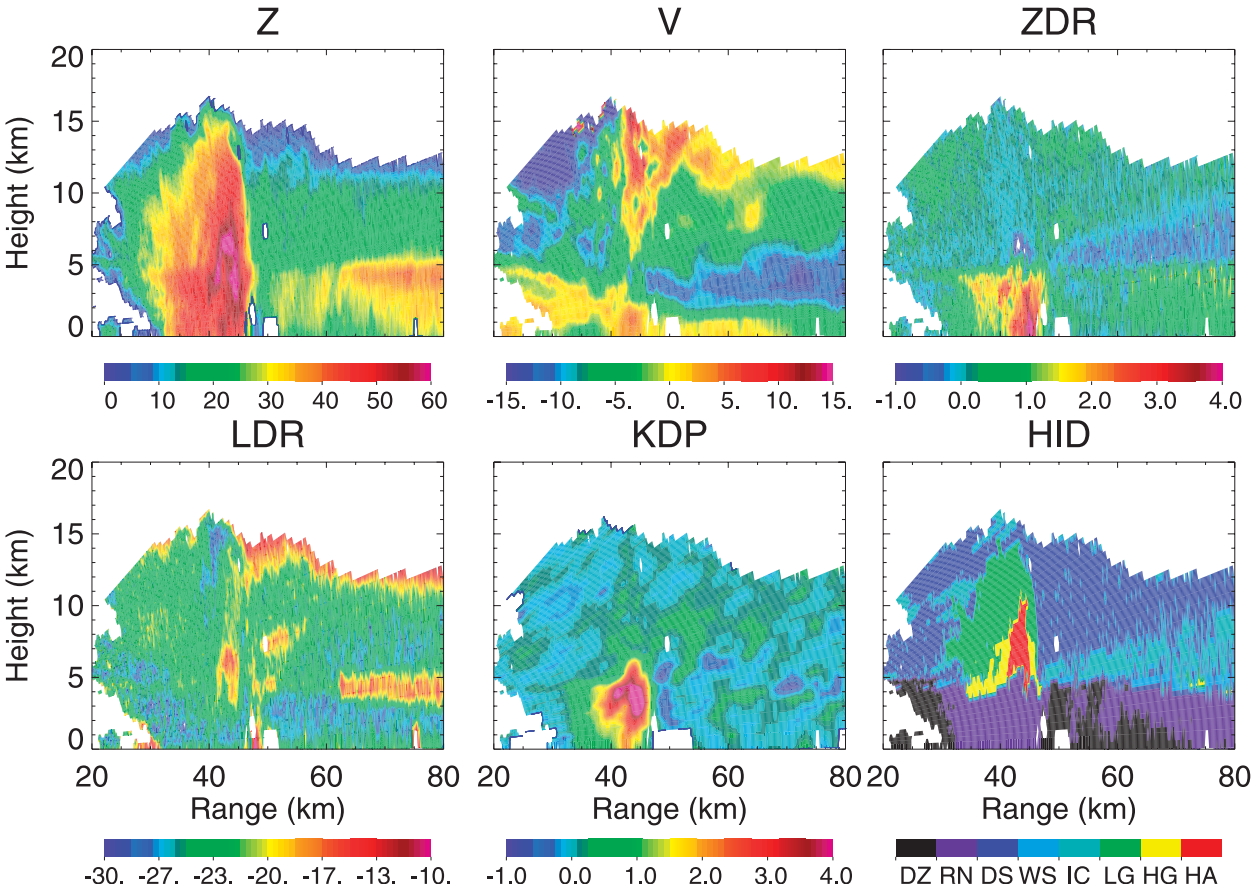

FIG. 5. An RHI through a cell at 2123 UTC 5 Aug 2004 at an azimuth of 96.6°. (from left to right starting at top) Variables include reflectivity (Z, dBZ), radial velocity (V_R, m s^{-1}), differential reflectivity (Z_{DR}, dB), linear depolarization ratio (L_{DR}, dB), specific differential phase (K_{DP}, ° km^{-1}), and the hydrometeor identification (HID). The HID abbreviations are the same as in Fig. 2.

radial velocity image at this time shows low-level upslope flow converging with downslope flow off the higher terrain, with the convergence zone collocated with the leading convective area. This flow pattern is consistent with a study by Johnson et al. (2010), who used surface and upper-air data during NAME to describe a reversal in the daytime, upslope flow along the SMO during the evening and overnight hours, leading to a westward-propagating zone of convergence that moved downslope toward the coast by early morning. An RHI at this time (96.6° azimuth; Fig. 5) highlights this newer leading convection following the decay of the older convective line. The combination of an elevated area of 60-dBZ reflectivity above the melting level along the back edge of the cell with negative Z_{DR} values and $L_{DR} > -21$ dB suggested the presence of hail in the wet growth stage (e.g., Balakrishnan and Zrnić 1990). Values of K_{DP} reached 4° km^{-1} below this region of hail due to melting, precipitation-sized ice hydrometeors. The velocity image at this time shows strong inbound velocities at midlevels converging with outbound velocities associated with the upslope flow. A relatively small area of inbound velocities at low levels indicated the production of outflow and promoted continued initiation of convection over the lower terrain.

Shortly after this time, as this system moved toward the coast, the radar no longer topped the convection moving toward the radar from the east, thereby limiting further analysis of the evolution of the vertical structure. However, at this same time, convection along the northern edge of the system continued to merge, persisting in an area of convergence along the coastal plain as surface winds to the north of this area had shifted from westerly to northerly. The MCS then began to move toward the northwest, moving parallel to the coast within this convergence zone. The system eventually passed over the S-band profiler to the north of S-Pol, where Lerach et al. (2010) noted characteristics of the stratiform region similar to MCSs in other regions of tropical precipitation (e.g., Williams et al. 1995; Ecklund et al. 1999; May and Keenan 2005), including a reflectivity brightband and strong Doppler velocity gradients within the melting layer.

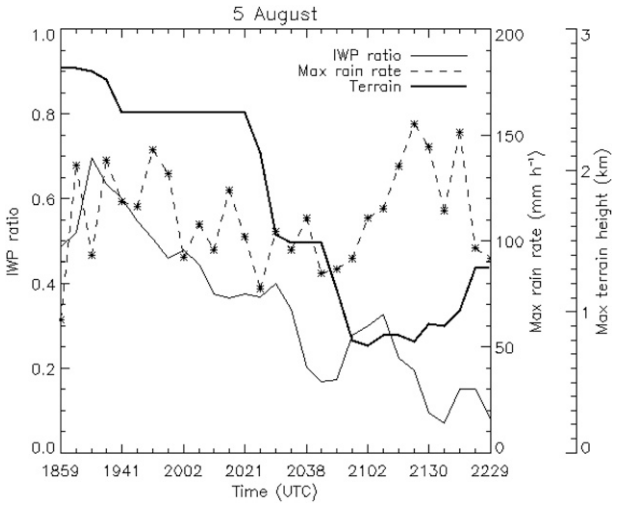

FIG. 6. A time series of IWP ratio and maximum rain rate (mm h^{-1}) associated with a cell track on 5 Aug 2004 as a function of terrain height.

This case, which captured the life cycle of an MCS during NAME from its origin over the SMO to the highly organized stage over low terrain, provided a unique opportunity to evaluate the evolution of an organized system as a function of topography. Vertical profiles of mean ice mass for all organized cells in this case (not shown) highlighted the deep extent of ice in cells over the lower terrain, as seen in the vertical cross sections; however, similar values existed in the mixed-phase region for all (terrain) elevations. A particular track, which captured the initiation of the cell over the SMO through organization over the lower terrain, demonstrated an expected general decrease in IWP ratio as the warm-cloud depth increased over the lower terrain (Fig. 6). This suggests that although a similar amount of ice mass was available in the mixed-phase region, the increased warm-cloud depth over the coastal plain allowed for an additional contribution to rainfall from coalescence compared to the SMO, similar to results presented by Rowe et al. (2008, 2011). Over the low terrain, the combined effects of ice-based and warm-rain processes led to rain rates exceeding 150 mm h^{-1}; however, maximum rainfall rates were consistently >100 mm h^{-1} for this track (Fig. 6), suggesting the importance of melting ice hydrometeors for rainfall production over the high terrain of the SMO.

b. 20–21 July

Similar to 5 August, convection initiated over the SMO during the afternoon of 20 July, another period of peak CAPE and vertical wind shear (Pereira 2008), later organizing into a quasi-linear MCS along the western slopes. The location of the monsoon anticyclone positioned the upper-level jet over the domain, leading to the increased wind shear. This, combined with upper-level diffluence ahead of an approaching upper-level

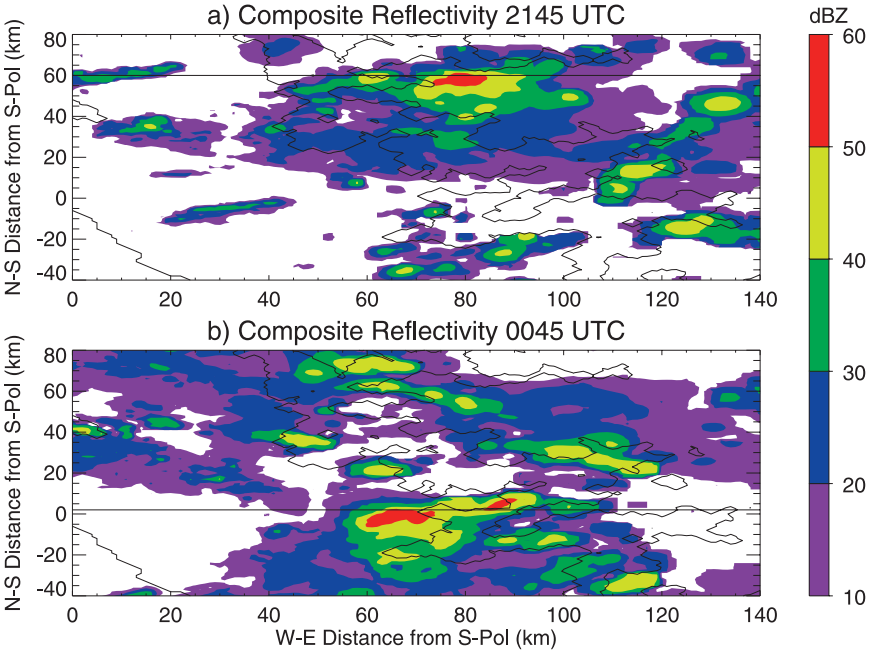

FIG. 7. As in Fig. 1, but for (a) 2145 UTC 20 Jul 2004 and (b) 0045 UTC 21 Jul 2004. Black lines show the location of cross sections in Fig. 8.

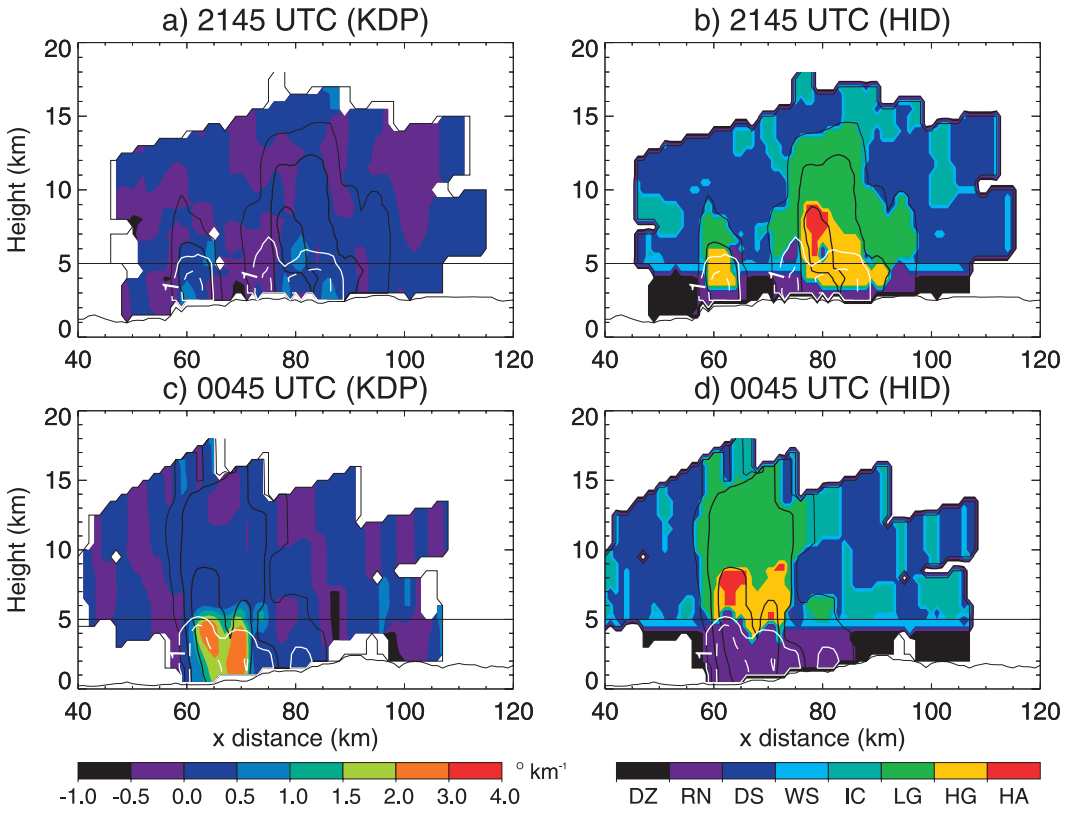

FIG. 8. Vertical cross sections through cells at (a),(b) 2145 UTC 20 Jul 2004 and (c),(d) 0045 UTC 21 Jul 2004. See Fig. 2 for a description of the variables and contours.

inverted trough and enhanced instability, provided favorable conditions for the development of larger-scale systems. However, unlike the previous case, this system weakened before moving out over the water as a result of reduced instability during the overnight hours; this strictly cross-coast movement led to the system being classified as regime A (Lang et al. 2007).

Scattered convection initiated over the high terrain around 2000 UTC, and, by 2145 UTC, had merged into larger clusters (Fig. 7a). A vertical cross section at this

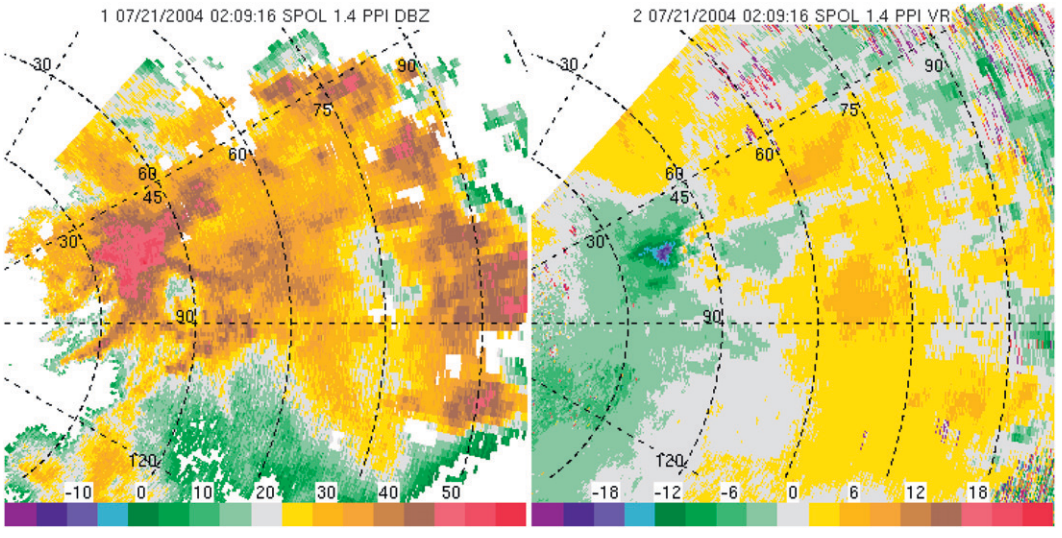

FIG. 9. PPI images of (left) reflectivity (dBZ) and (right) radial velocity (m s^{-1}) at 0209 UTC 21 Jul 2004 at 1.4°.

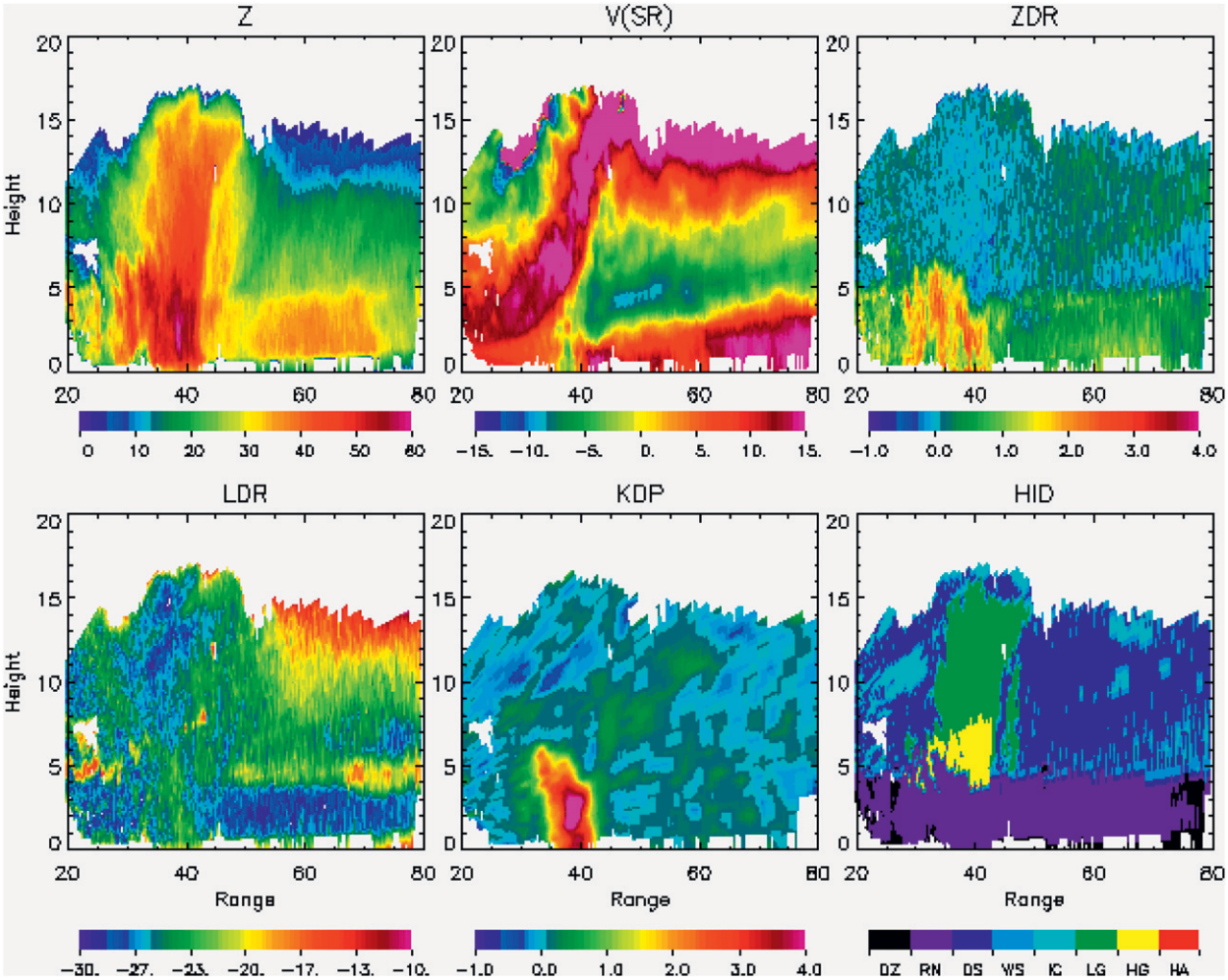

FIG. 10. An RHI through a cell at 0208 UTC 21 Jul 2004 at an azimuth of 75°. Variables are as described in Fig. 5, except that velocity in this figure is storm relative.

time (Figs. 8a,b) highlights deep convection extending to nearly 18 km, with graupel and hail reaching 9 km (Fig. 8b), a Z_{DR} column present along the leading edge near the 75-km range, yet K_{DP} values below the melting level of $<1°$ km^{-1}, likely due to a reduced warm-cloud depth limiting liquid water content. However, over the next several hours, this convective area decayed without further organization while additional convection developed due east of the radar along the foothills in a convergence zone between upslope and downslope flow. A vertical cross section through this newer, growing convective area at 0045 UTC (Fig. 7b) highlights a deep cell with a similar vertical extent of large ice hydrometeors as the previous cross section (Fig. 8d), although it has a greater warm-cloud depth with larger K_{DP} and Z_{DR} values (Fig. 8c), suggesting the presence of larger drops and higher liquid water contents. All variables plotted in these cross sections also highlight the multicellular nature of this system via two separate cores: an older, decaying core near the 70-km range with $K_{DP} > 2°$ km^{-1} extending to the surface (Fig. 8c) accompanied by a small region of hail identified by the HID (Fig. 8d), and a newer core between the 60- and 65-km range characterized by an elevated maxima in K_{DP} (Fig. 8c), a larger hail area (Fig. 8d), and a greater vertical extent of positive Z_{DR}.

With time, the leading edge continued to move off the terrain toward the radar along the convergence zone and older convection continued to decay, contributing to the stratiform precipitation back over the higher elevations (Fig. 9). The velocity plan position indicator (PPI) in this figure, in addition to the convergence, also shows an enhanced pocket of inbound velocities along the leading edge of the convection, suggesting the production of outflow. An RHI through the MCS at this time (0208 UTC; 75° azimuth; Fig. 10) reveals storm-relative,

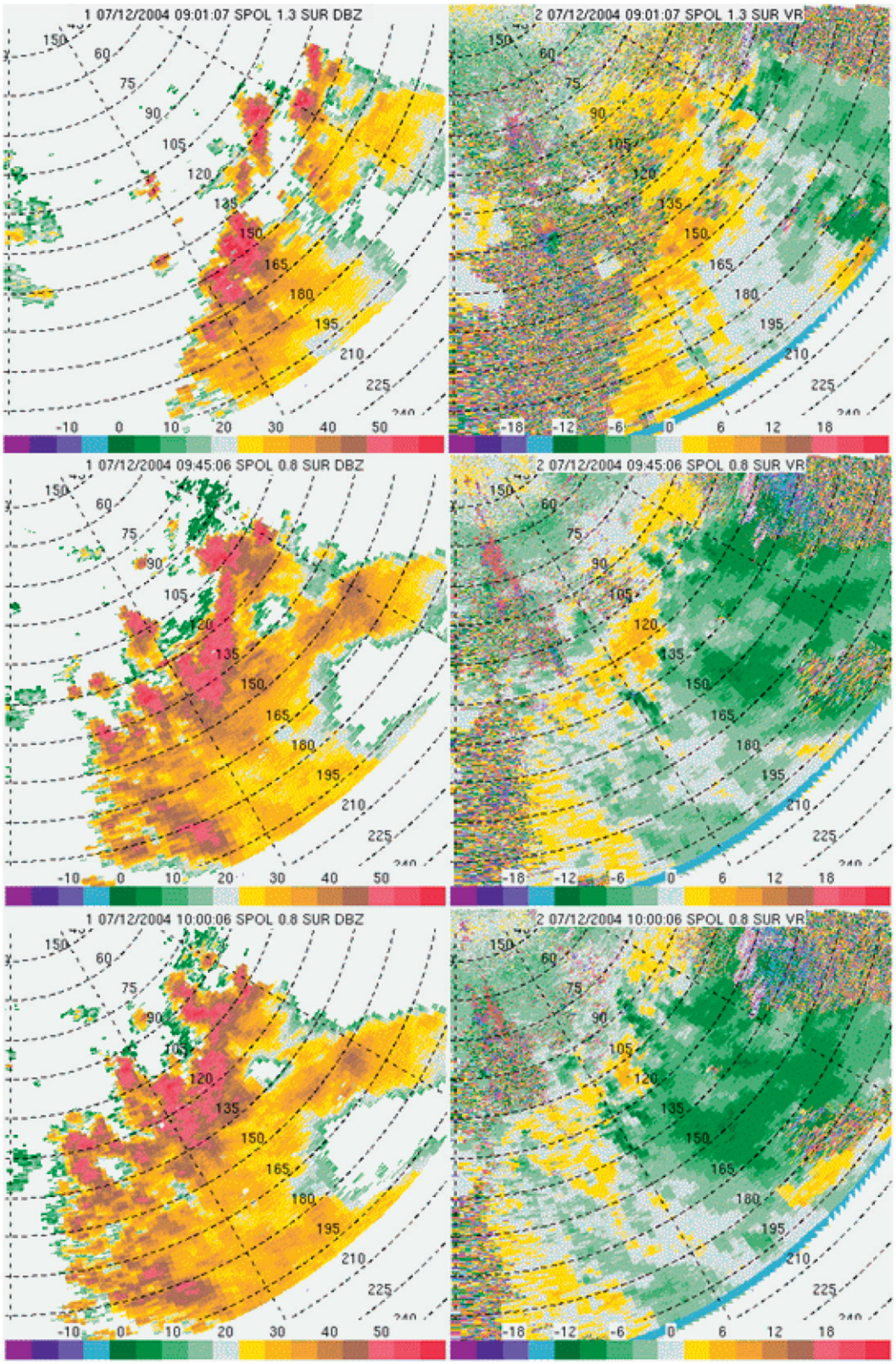

FIG. 11. PPI images of (left) reflectivity (dBZ) and (right) radial velocity (m s^{-1}) for (top) 0901 UTC (1.4°), (middle) 0945 UTC (0.8°), and (bottom) 1000 UTC (0.8°) 12 Jul 2004.

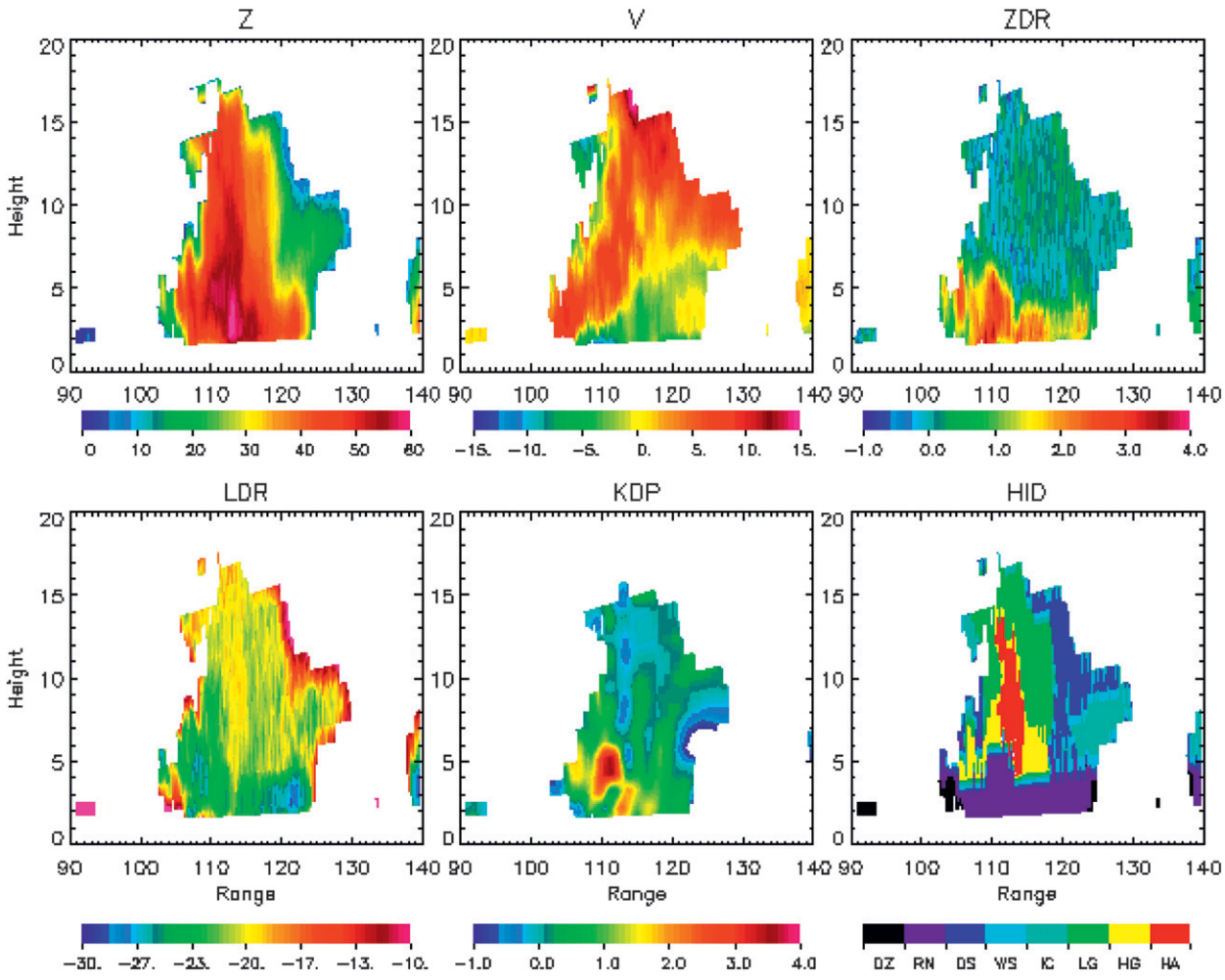

FIG. 12. An RHI through a cell at 0912 UTC 12 Jul 2004 at an azimuth of 126°. Variables are as described in Fig. 5.

midlevel rear inflow in the stratiform region of about 10 m s^{-1} that entered the system above the melting level between 5 and 8 km and descended to near the surface as it approached the leading convective line. Descending rear inflow, combined with convective downdrafts within the precipitation core, results in the enhancement of cold pools, which propagate away from the leading line and initiates new convection. The strength of the cold pool is related to microphysical processes through convective downdrafts via precipitation loading, evaporation, and melting of ice hydrometeors (e.g., Knupp and Cotton 1985; Srivastava 1985, 1987). In particular, van den Heever and Cotton (2004) noted that the melting of small hailstones in supercells resulted in strong low-level downdrafts and deeper, faster-moving cold pools, further suggesting an important role of melting in the production and modification of cold pools. Elevated maxima in polarimetric variables observed under the HID-identified graupel region (Fig. 10) suggest melting of these large ice hydrometeors (i.e., graupel, hail), and storm-relative velocities show a localized area of inbound velocities near the surface beneath the core indicating the presence of outflow, which are consistent with these studies and likely leading to the new convective initiation at closer ranges (between 20 and 30 km). Keenan and Carbone (1992) also noted the importance of a spreading cold pool for initiation of new convection in tropical systems in northern Australia. Similar processes were found within MCSs over the Himalayas, where Medina et al. (2010) described the merging of strong convection along the foothills and development of cold pools that led to new convective initiation over the lower terrain as these boundaries converged with the monsoonal (upslope) flow.

Ice physics also play a role in the stratiform region, controlling the latent heat distribution and thus the flow pattern resulting from pressure gradients. Numerical

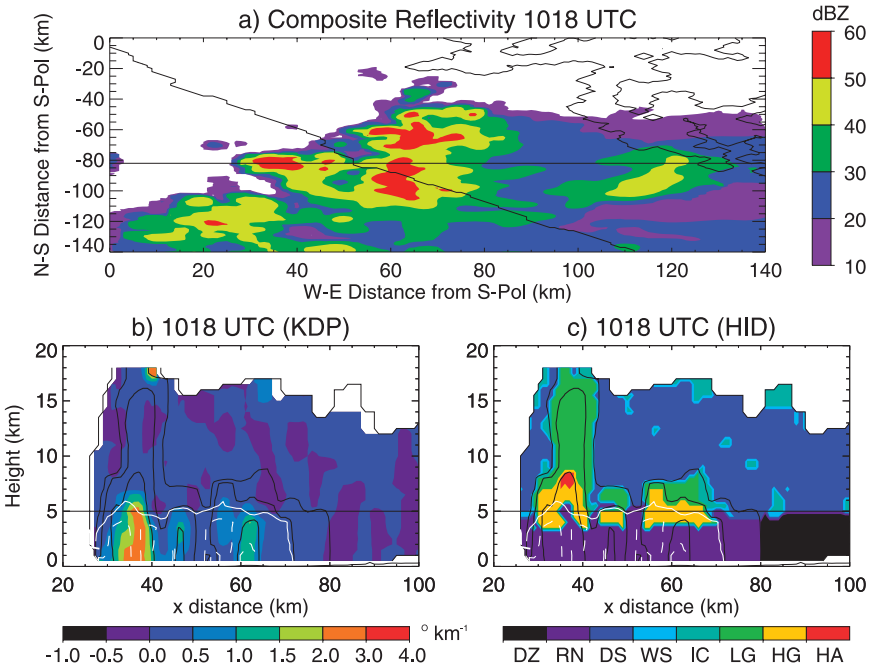

FIG. 13. (a) Gridded composite reflectivity for 1018 UTC 12 Jul 2004. (b),(c) Vertical cross sections with contours as described in Fig. 2. The black line in (a) indicates the location of the vertical cross sections.

simulations of tropical MCSs in western Africa noted that experiments, which did not include ice, produced less organized systems in which the rear inflow was weaker and did not reach the ground, thereby eliminating the surface gust front (Liu et al. 1997). The generation of outflow also depended on the mass flux in convective downdrafts, with enhancements observed when the ice phase was included. Therefore, the presence of precipitation-sized ice, rear inflow, and outflow boundaries in these NAME cases suggests a likely dependence of organization on microphysical processes.

c. 12 July

While the previous cases focused on convective organization along the terrain within the range of S-Pol, this example, which occurred from 0700 to 1300 UTC 12 July 2004, highlights an MCS that moved into the domain from the southeast during the overnight hours. This period was characterized by moisture advection into the region as a result of enhanced east-southeast flow on the equatorward side of an anticyclone (Pereira 2008). Increased precipitable water led to an enhancement of CAPE with values exceeding 2000 J kg^{-1}, and the approach of an inverted trough increased the midlevel flow and, therefore, wind shear, providing favorable conditions for upscale growth (Finch and Johnson 2010). Convection initiated over the SMO between Mazatlan and Puerto Vallarta at 0300 UTC, and by 0500 UTC, began to organize as it moved off the higher terrain. At 0700 UTC, the leading edge of this system moved into the far southeastern portion of the S-Pol domain. Of the 996 individual cells identified and tracked during this case, 78% were considered part of organized systems, with 76% of those over the gulf and the remaining over land; therefore, the focus of this case will be on comparing convection over land with that over water.

At 0900 UTC, convection extended from the coast to over the western slopes of the SMO along an area of convergence with stratiform trailing behind (Fig. 11a). An RHI through this leading convection at 0912 UTC (126° azimuth; Fig. 12) highlights a deep cell with the echo top reaching 17 km, 50-dBZ reflectivities to 15 km, and a mixture of high-density graupel and hail extending to 14 km. Melting of these large ice hydrometeors can be inferred by K_{DP} near 4° km^{-1} and Z_{DR} of 4 dB just below the melting level. The development of a new core is evident along the leading edge between 105- and 110-km range, with positive Z_{DR} extending above the melting level within an elevated area of higher K_{DP} and graupel. The velocity image shows storm-top divergence and ground-relative, low-level flow toward the radar associated with storm outflow. This outflow can be seen in the PPI image at 0945 UTC as an arc of lower reflectivities (Fig. 11b; 120°–130° at the 90-km range) ahead of the leading line. By the next time (1000 UTC;

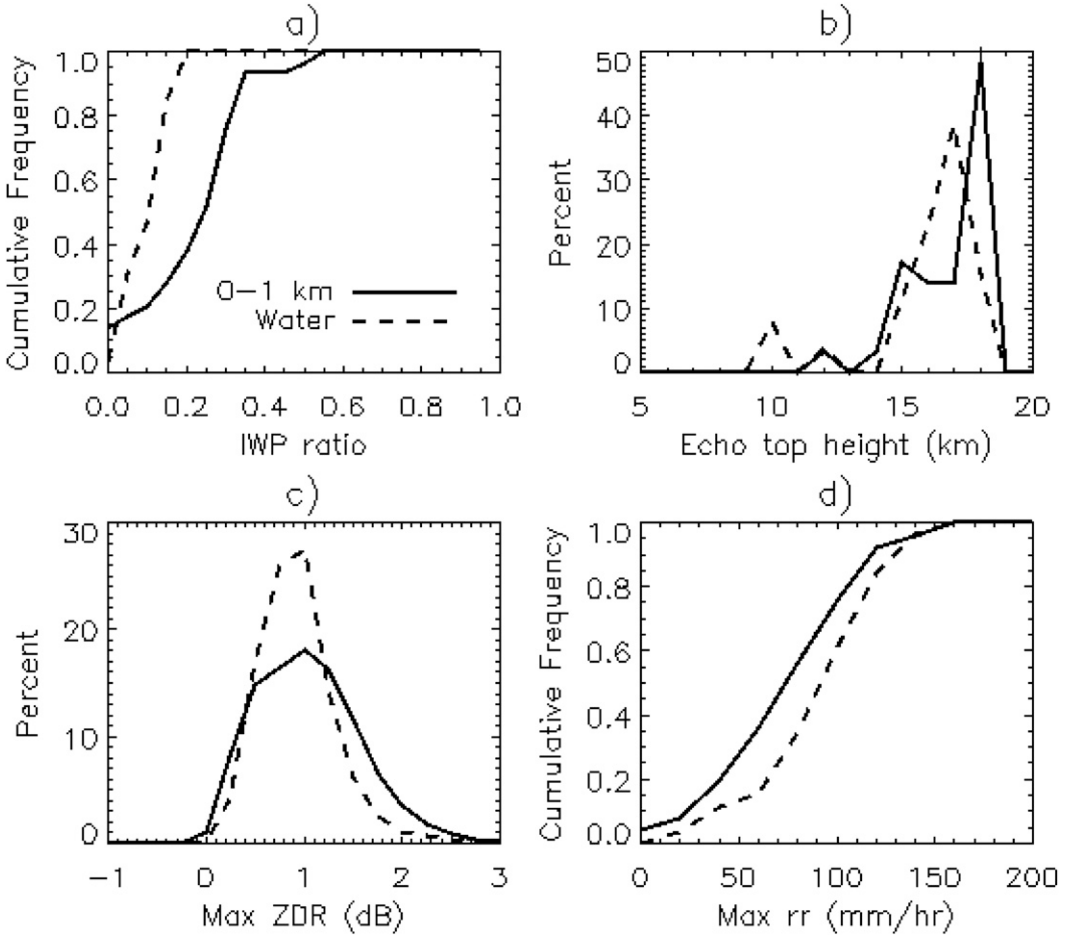

FIG. 14. Distributions associated with a track over the low terrain (0–1 km) and with a track over water on 12 Jul 2004. Plotted variables represent values associated only with cells in these particular tracks.

Fig. 11c), convection had initiated along this boundary, further emphasizing the importance of outflow boundaries for storm maintenance and propagation in this region.

New convection continued to initiate along these boundaries over the lower terrain and adjacent waters of the Gulf of California. A vertical cross section at 1018 UTC through a portion of the system over the gulf (Fig. 13a) shows deep convection along the leading edge over water, characterized by reflectivity values of 40 dBZ extending to 16 km, $K_{DP} > 2^{\circ}$ km^{-1} (Fig. 13b), and graupel identified to near the echo top (Fig. 13c). Older cells continued to decay farther back near the coastline, contributing to trailing stratiform precipitation, as was also observed in the previously described cases.

Convective initiation continued through the next hour, suggesting the importance of outflow boundaries in the maintenance and propagation of the MCS as it moved offshore. The cell identification and tracking algorithm used in this study allowed for a comparison of cell characteristics between a track over land that followed a cell along the leading edge of the MCS as it moved toward the coast (29 cells; labeled 0–1 km in Fig. 14) with a track over water that followed the evolution of a cell that formed along an outflow boundary and moved farther away from the coast (26 cells; labeled water in Fig. 14). A comparison between IWP ratios (Fig. 14a), in particular, revealed that cells within the leading edge over the coastal plain contained more ice relative to the cells that initiated over water. Echo-top heights were also greater for the convection over land (Fig. 14b), possibly leading to the greater IWP ratios due to the greater depth over which ice could exist. The leading convection over the coastal plain also contained larger drops, as indicated by the wider Z_{DR} distribution compared to the track over water in Fig. 14c. However, despite the reduced ice mass, shallower echo tops, and smaller drops, the convection that occurred over the gulf had greater maximum rain rates (Fig. 14d) and larger K_{DP} (not shown), suggesting a significant contribution

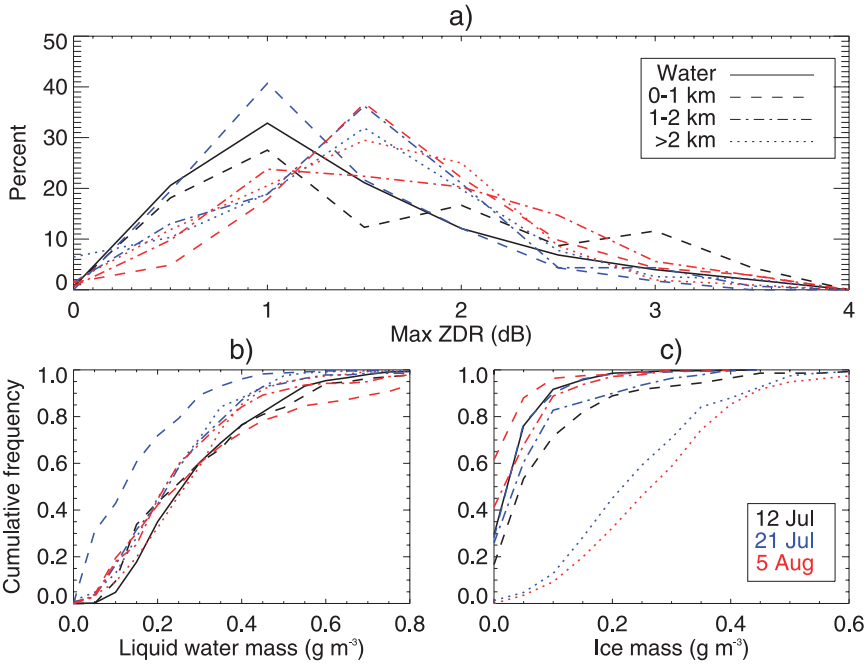

FIG. 15. Distributions for all organized cells identified during the specific case days. Liquid water and ice masses are normalized by cell volume.

from warm-rain processes. This is consistent with the Lang et al. (2010) study, where fundamental differences in drop size distributions were described between the land and water, including a tendency for convection over the gulf to contain smaller drops and less ice mass.

d. Case comparison

The cases presented herein are considered to represent the spectrum of organized systems that were observed by S-Pol during NAME. In every case examined, afternoon convection over the high terrain of the SMO gave way to an organized system over lower elevations. Although many systems dissipated before reaching the coast (e.g., 21 July), others persisted into the overnight hours (e.g., 5–6 August). In contrast to this cross-coast movement, some MCSs, such as the one described from 12 July, moved northwestward into the radar domain, thereby characterized by a longer residence time over water.

Distributions of maximum Z_{DR} within organized cells on these case days (Fig. 15a) show that drops were, on average, smallest over the coastal plain and adjacent gulf on 12 July, suggesting more maritime characteristics (e.g., Atlas and Ulbrich 2000; Bringi et al. 2003, 2009; Rosenfeld and Ulbrich 2003; Atlas and Ulbrich 2006; Ulbrich and Atlas 2007). Despite containing smaller drops, liquid water mass (Fig. 15b) was generally greatest for cells on this day, especially compared to cells over land on 21 July, consistent with the hypothesized greater dependence on warm-rain processes for systems moving over the gulf from the southeast. This is further supported by the cumulative distribution functions (CDFs) of ice mass (Fig. 15c), which show reduced ice mass over water, with the greatest amounts for cells over the SMO on 21 July and 5 August, indicating the importance of ice-phase processes in convection over the terrain.

4. Comparison with isolated convection

The previous case studies described the evolution of MCSs during NAME, composed of deep, intense convective elements that exhibited similar characteristics as isolated convection in this region, including Z_{DR} columns, large ice hydrometeors aloft, and an elevation dependence in microphysical processes (Rowe et al. 2011). Despite the greater frequency of isolated convection during NAME (Pereira 2008; Rowe et al. 2011), the long-lived MCSs were responsible for 75% of the total rainfall in the radar domain (Lang et al. 2007). The number of individual isolated cells was similar to the number of organized cells collected during the microphysical scans (6568 and 6908, respectively), allowing for meaningful comparisons; however, the majority of isolated cells occurred over the high terrain of the SMO (>2 km), whereas most organized convection was located over the western slopes (1–2 km) and coastal plain (0–1 km). Therefore, to provide a more accurate comparison, isolated and organized cells were further subdivided based on elevation.

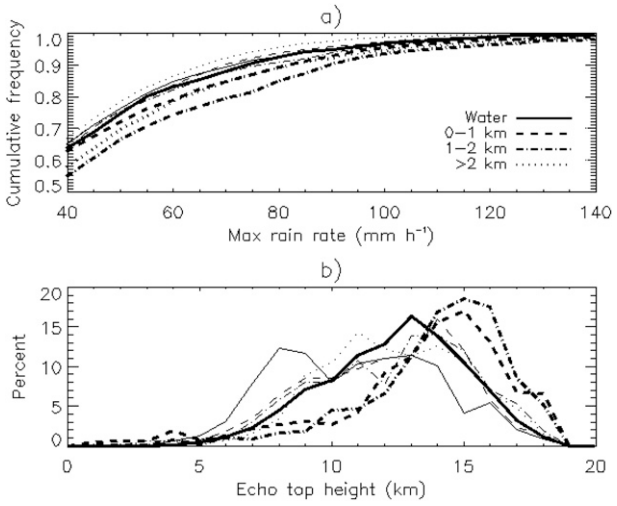

FIG. 16. Comparison between isolated (thin lines) and organized (thick lines) convection for all cells identified within the S-Pol microphysical scans. Note that the axes for cumulative frequencies of maximum rain rate are truncated to focus on higher rainfall intensities.

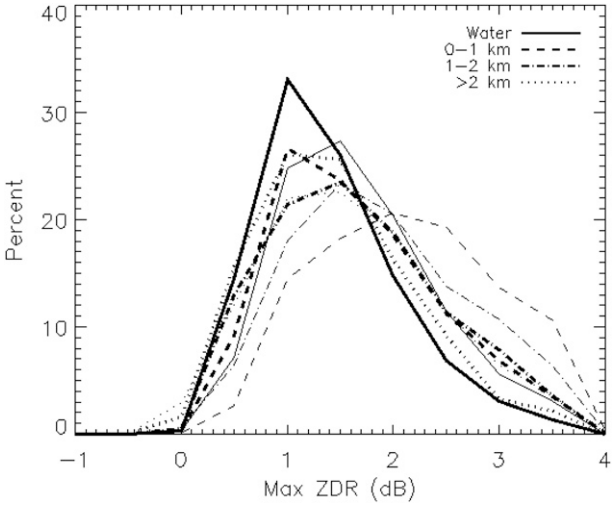

FIG. 17. Distribution of maximum Z_{DR} for all cells within the microphysical scans, divided into isolated (thin lines) and organized (thick lines) cells, and further subdivided by elevation group. Percent represents the percentage for the specified type and elevation category.

CDFs of maximum rain rate (Fig. 16a), grouped by feature type and elevation, show greater rainfall intensity for cells contained within MCSs, suggesting that increased intensity was at least partly responsible for greater precipitation totals associated with organized systems in this region. Maximum instantaneous rain rates were associated with organized convection along the western slopes, consistent with the tendency for the most intense rainfall to occur during the late afternoon/early evening over the lower elevations of the SMO (Rowe et al. 2008). A direct relationship existed between storm depth and rain rates for isolated cells (Rowe et al. 2011); therefore, it is no surprise that echo-top heights were generally higher for organized convection regardless of terrain height (Fig. 16b), especially given the similar CAPE values on each day (Pereira 2008). Similar results were found using radar data from the Tropical Ocean Global Atmosphere Coupled Ocean–Atmosphere Response Experiment (TOGA COARE), where mesoscale systems contributed 80% of rainfall during the experiment despite a greater frequency of isolated cells, and the tallest echo-top heights were associated with organized convection (Rickenbach and Rutledge 1998). Although the population sample was comparatively small, organized systems during NAME tended to be shallower over the water compared to land for both organized and isolated convection (Fig. 16b), which is consistent with observations presented in the previous cases.

To further investigate differences in microphysical characteristics, distributions of maximum Z_{DR} within cells were grouped by feature type and topography (Fig. 17). Overall, for a given range of topography, there was a tendency for isolated cells to have larger Z_{DR} values compared to organized convection. In particular, isolated cells over the lower elevations contained the largest drops and widest distribution compared to the cells embedded within organized systems over the coastal plain and adjacent water. Organized convection over the slopes, where rainfall rates were maximized, was characterized by greater Z_{DR} values compared to cells embedded within MCSs over the lower terrain and gulf, suggesting a greater contribution from melting ice hydrometeors to rainfall. Frequency contours of K_{DP} as a function of Z_{DR} are presented for isolated and organized convection over the 0–1-km elevation range (Figs. 18a,b). Both figures show the occurrence of Z_{DR} values exceeding 4 dB, yet for lower Z_{DR} (i.e., 1–2 dB, drop sizes ranging from roughly 1.5–2 mm), K_{DP} values were greater for cells embedded within organized systems, indicating higher liquid water contents. This suggests that although large drops were present in both isolated and organized convection, the presence of higher concentrations of smaller drops in organized convection may have contributed to the enhanced rainfall associated with these systems. The shift in the drop size distribution is even more evident when comparing these frequencies between organized convection over land compared to that over water (Figs. 18c,d), which show that large K_{DP} was limited to lower Z_{DR} values over the gulf, characteristic of more maritime-like systems (e.g., 12 July).

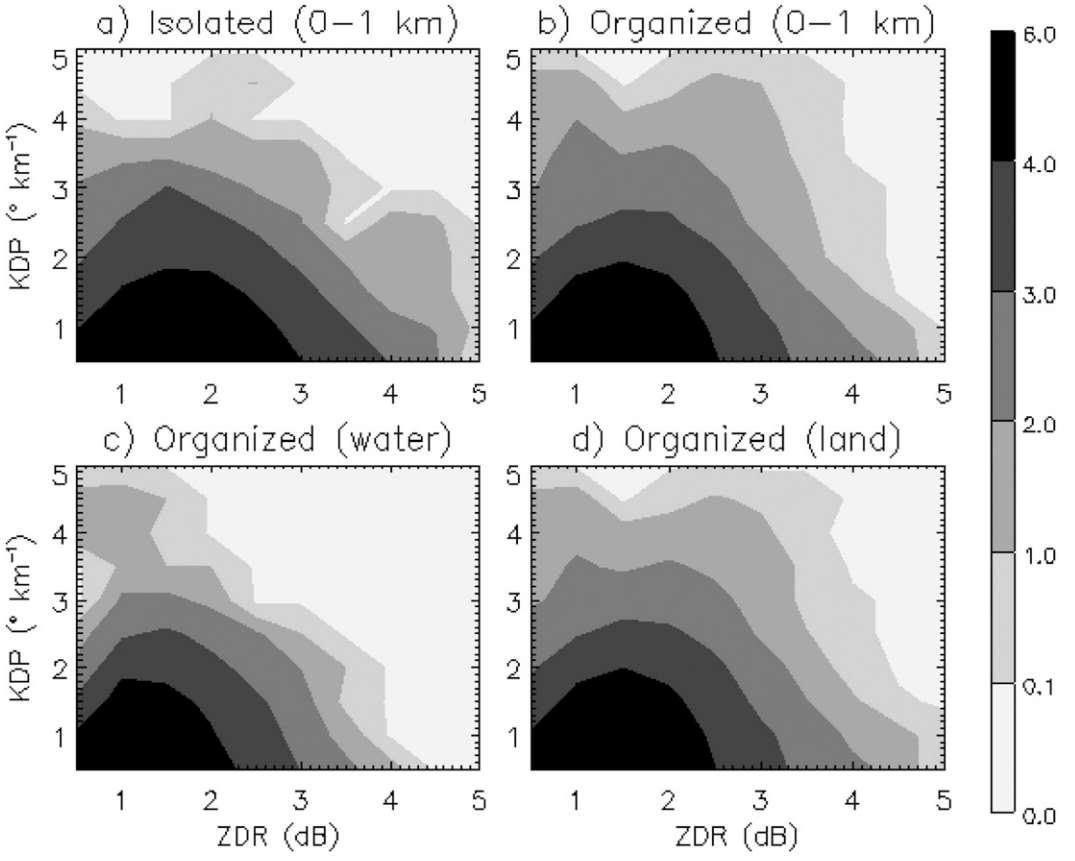

FIG. 18. Contoured frequencies of K_{DP} as a function of Z_{DR} for (a) isolated cells over low terrain (0–1 km), (b) organized cells over low terrain (0–1 km), (c) organized cells over water, and (d) organized cells over land (all elevations). Only values identified as rain by the HID and located below 4 km are considered. Plotted are the logarithms of frequencies normalized by the total frequency in the specified elevation grouping.

Vertical profiles of mean ice mass within a cell (Fig. 19a) show greater ice mass in organized cells over the higher elevations compared to the coastal plain, further implying an important role of ice-based processes in producing heavy rainfall over the terrain. In addition, MCS convection generally contained higher ice mass compared to isolated convection over land, especially within the mixed-phase region near 6 km, with the exception of the intense, isolated cells over the SMO captured by the microphysical scans. This smaller change in ice mass with organization over the SMO, compared to other elevations, is consistent with previous NAME studies that found little day-to-day variability in precipitating systems over the high terrain (Lang et al. 2007, 2010; Nesbitt et al. 2008). Furthermore, there was a trend of reduced ice mass over water compared to that over land, similar to results found for all S-Pol-detected cells during NAME (Lang et al. 2010), and as described in the case studies presented herein. Vertical profiles of mean liquid water mass (Fig. 19b) reveal a trend in which greater amounts of liquid water were present below the melting level for MCS convection compared to isolated cells, consistent with the abundance of small drops in organized convection shown in Fig. 18, in addition to the larger amounts of ice falling out and melting.

In general, convection in organized systems was characterized by greater rain rates, in addition to longer life spans, with taller echo-top heights and greater water and ice masses compared to isolated cells. Isolated cells had larger Z_{DR} values, especially compared to organized systems over the lower terrain and gulf, which contained larger concentrations of smaller drops and led to increased liquid water mass in the low levels. This apparent dependence of intensity on organization is also likely due to the more favorable environmental conditions under which MCSs develop. Intense rainfall associated with organized systems during NAME occurred during periods of both enhanced CAPE and shear (Pereira 2008), consistent with studies of heavy rain-producing MCSs during TOGA COARE (Lucas and Zipser 2000). The relative contributions of the mesoscale dynamics inherent to the organized systems and

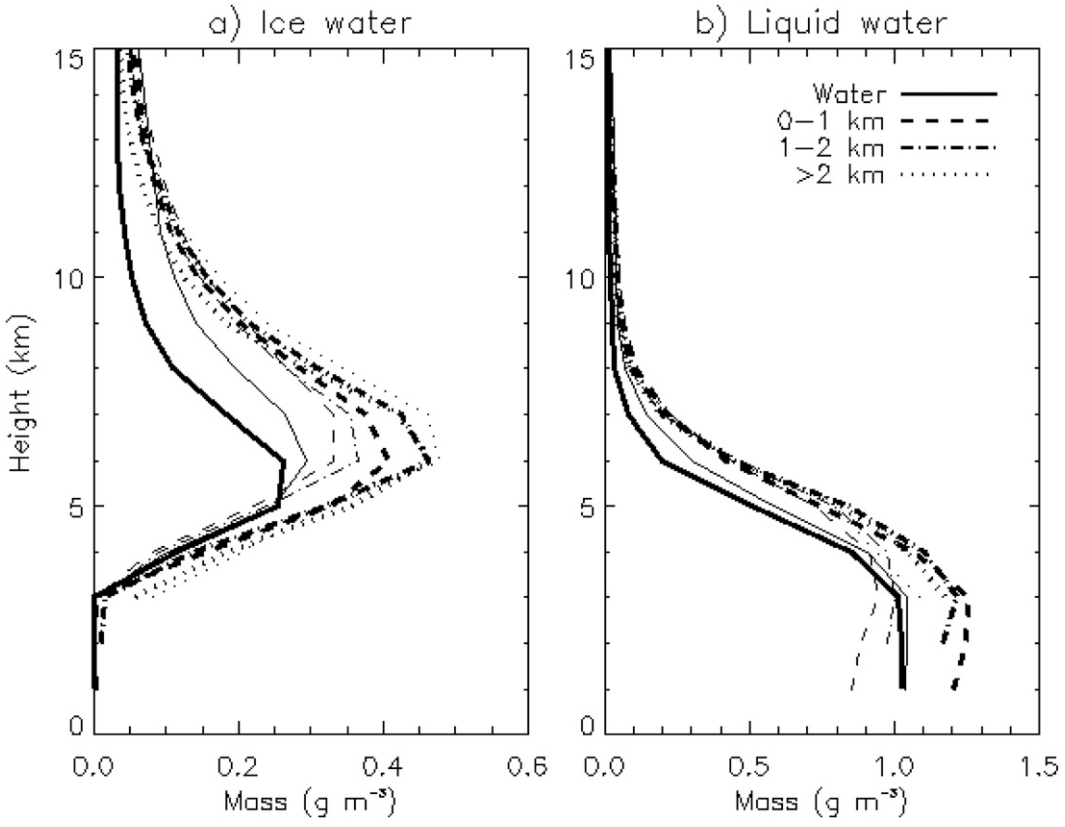

FIG. 19. Profiles of mean (a) ice and (b) liquid water masses for all isolated (thin lines) and organized (thick lines) cells within the microphysical scans, categorized by elevation group.

the favorable large-scale environmental conditions to the enhanced rainfall associated with MCSs during NAME are topics beyond the scope of this study.

5. Discussion and summary

A major objective of NAME was to describe the microphysical processes of convection relative to the significant terrain variations in that region. Previous work by Rowe et al. (2011) compared examples of isolated convection, but despite the high frequency of occurrence of isolated cells during NAME, organized systems were responsible for 75% of rainfall in the radar domain. Compared to isolated convection, cells embedded within MCSs were characterized by larger rain rates, taller echo-top heights, and greater liquid and ice mass. Maritime-like drop size distributions (i.e., greater concentrations of smaller drops) were more evident within organized convection over the gulf, where systems moving into the domain from the south had longer residence times over water (e.g., 12 July). Greater warm-cloud depths over the water and lower elevations suggested a significant contribution from warm-rain processes, but the importance of mixed-phase processes was also inferred due to observations of Z_{DR} columns within the leading convective lines of three MCS cases examined in this study. Along with this signature, the collapse of older cells to maintain the trailing stratiform region in those cases highlighted similarities to MCSs in the midlatitudes (Houze 1993, 1997).

Examples of convection organizing along the western slopes demonstrated differences in microphysical processes as a function of elevation. Deep convection initiated over the SMO during the afternoon hours containing comparable amounts of ice mass observed in cells over lower elevations. With time, this convection organized into MCSs, characterized by a leading line with trailing stratiform consisting of older, dissipating cells. The frequent occurrence of elevated maxima in K_{DP} and Z_{DR} highlighted the important role of melting ice in producing rainfall along the western slopes. This melting, in addition to descending rear inflow, led to the development of outflow boundaries, which spread over the lower elevations and converged with the larger-scale upslope flow, leading to new convective development. Once over lower elevations, additional warm-cloud

depth aided in the production of intense, long-lasting rainfall, Combined with a favorable unstable environment, production of large ice continued, which melted, sustained convective outflow, and contributed to the propagation of these systems away from higher elevations. This occurrence of organized systems upstream of and over lower elevations has also been noted in other mountainous regions, including the Himalayas (Medina et al. 2010), the western Ghats (Grossman and Durran 1984), the European Alps (Houze et al. 2001), and the Pyrenees (Romero et al. 2001).

Because of the apparent importance of microphysics and cold pools in the organization and propagation of MCSs in the NAME region, the understanding of hydrometeor characteristics described in this study should prove useful not only for convective parameterization schemes, but also for the simulation of cold pool dynamics. In addition, the cases described in this study were characterized by environments with increased CAPE and vertical wind shear; therefore, the effect of the interaction between the cold pools and these environmental conditions on organization will need to be further investigated in order to properly simulate the MCS life cycle and feedbacks to the monsoon circulation via heat and momentum transport.

Acknowledgments. We thank those who contributed to the successful deployment of S-Pol during NAME and the subsequent quality control of the data, including Rit Carbone, Dave Ahijevych, Bob Rilling, Chad Christenson, Lee Nelson, and Gustavo Pereira. This work greatly benefitted from the development of the cell-tracking algorithm by Lee Nelson and Dr. Steven Nesbitt. This research was funded by the National Science Foundation Grant ATM-0733396.

REFERENCES

Atlas, D., and C. W. Ulbrich, 2000: An observationally based conceptual model of warm oceanic convective rain in the Tropics. *J. Appl. Meteor.,* **39,** 2165–2181.

——, and ——, 2006: Drop size spectra and integral remote sensing parameters in the transition from convective to stratiform rain. *Geophys. Res. Lett.,* **33,** L16803, doi:10.1029/2006GL026824.

Balakrishnan, N., and D. S. Zrnić, 1990: Use of polarization to characterize precipitation and discriminate large hail. *J. Atmos. Sci.,* **47,** 1525–1540.

Bluestein, H. B., and M. H. Jain, 1985: Formation of mesoscale lines of precipitation: Severe squall lines in Oklahoma during the spring. *J. Atmos. Sci.,* **42,** 1711–1732.

Bringi, V. N., and V. Chandrasekar, 2001: *Polarimetric Doppler Weather Radar Principles and Applications*. Cambridge University Press, 636 pp.

——, ——, J. Hubbert, E. Gorgucci, W. L. Randeu, and M. Schoenhuber, 2003: Raindrop size distribution in different climatic regimes with disdrometer and dual-polarized radar analysis. *J. Atmos. Sci.,* **60,** 354–365.

——, C. R. Williams, M. Thurai, and P. T. May, 2009: Using dual-polarized radar and dual-frequency profiler for DSD characteristics: A case study from Darwin, Australia. *J. Atmos. Oceanic Technol.,* **26,** 2107–2122.

Carey, L. D., and S. A. Rutledge, 2000: The relationship between precipitation and lightning in tropical island convection: A C-band polarimetric radar study. *Mon. Wea. Rev.,* **128,** 2687–2710.

Cifelli, R., W. A. Petersen, L. D. Carey, S. A. Rutledge, and M. A. F. Silva-Dias, 2002: Radar observations of the kinematic, microphysical, and precipitation characteristics of two MCSs in TRMM LBA. *J. Geophys. Res.,* **107,** 8077, doi:10.1029/2000JD000264.

——, V. Chandrasekar, S. Lim, P. C. Kennedy, Y. Wang, and S. A. Rutledge, 2011: A new dual-polarization radar rainfall algorithm: Application in Colorado precipitation events. *J. Atmos. Oceanic Technol.,* **28,** 352–364.

Dai, A. G., F. Giorgi, and K. E. Trenberth, 1999: Observed and model-simulated diurnal cycles of precipitation over the contiguous United States. *J. Geophys. Res.,* **104** (D6), 6377–6402.

Douglas, M., R. A. Maddox, K. Howard, and S. Reyes, 1993: The Mexican monsoon. *J. Climate,* **6,** 1665–1677.

Doviak, R. J., and D. S. Zrnić, 1993: *Doppler Radar and Weather Observations*. 2nd ed. Academic Press, 562 pp.

Ecklund, W. L., C. R. Williams, P. E. Johnston, and K. S. Gage, 1999: A 3-GHz profiler for precipitating cloud studies. *J. Atmos. Oceanic Technol.,* **16,** 309–322.

Finch, Z. O., and R. H. Johnson, 2010: Observational analysis of an upper-level inverted trough during the 2004 North American Monsoon Experiment. *Mon. Wea. Rev.,* **138,** 3540–3555.

Gochis, D. J., W. J. Shuttleworth, and Z. L. Yang, 2002: Sensitivity of the modeled North American monsoon regional climate to convective parameterization. *Mon. Wea. Rev.,* **130,** 1282–1298.

——, A. Jimenez, C. J. Watts, J. Garatuza-Payan, and W. J. Shuttleworth, 2004: Analysis of 2002 and 2003 warm-season precipitation from the North American Monsoon Experiment Event Rain Gauge Network. *Mon. Wea. Rev.,* **132,** 2938–2953.

——, C. J. Watts, J. Garatuza-Payan, and J. Cesar-Rodriguez, 2007: Spatial and temporal patterns of precipitation intensity as observed by the NAME event rain gauge network from 2002 to 2004. *J. Climate,* **20,** 1734–1750.

Grossman, R. L., and D. R. Durran, 1984: Interaction of low-level flow with the Western Ghat mountains and offshore convection in the summer monsoon. *Mon. Wea. Rev.,* **112,** 652–672.

Hall, M. P. M., J. W. F. Goddard, and S. M. Cherry, 1984: Identification of hydrometeors and other targets by dual-polarization radar. *Radio Sci.,* **19,** 132–140.

Higgins, R. W., and Coauthors, 2006: The NAME 2004 field campaign and modeling strategy. *Bull. Amer. Meteor. Soc.,* **87,** 79–94.

Houze, R. A., Jr., 1993: *Cloud Dynamics*. Academic Press, 573 pp.

——, 1997: Stratiform precipitation in regions of convection: A meteorological paradox? *Bull. Amer. Meteor. Soc.,* **78,** 2179–2196.

——, C. N. James, and S. Medina, 2001: Radar observations of precipitation and airflow on the Mediterranean side of the Alps: Autumn 1998 and 1999. *Quart. J. Roy. Meteor. Soc.,* **127,** 2537–2558.

Illingworth, A. J., J. W. F. Goddard, and S. M. Cherry, 1987: Polarization radar studies of precipitation development in convective storms. *Quart. J. Roy. Meteor. Soc.,* **113,** 469–489.

Johnson, R. H., P. E. Cielsielski, T. S. L'Ecuyer, and A. J. Newman, 2010: Diurnal cycle of convection during the 2004 North American Monsoon Experiment. *J. Climate,* **23,** 1060–1078.

Keenan, T. D., and R. E. Carbone, 1992: A preliminary morphology of precipitation systems in tropical northern Australia. *Quart. J. Roy. Meteor. Soc.,* **118,** 283–326.

Knupp, K. R., and W. R. Cotton, 1985: Convective cloud downdraft structure: An interpretive survey. *Rev. Geophys.,* **23,** 183–215.

Lang, T. J., D. A. Ahijevych, S. W. Nesbitt, R. E. Carbone, S. A. Rutledge, and R. Cifelli, 2007: Radar-observed characteristics of precipitating systems during NAME 2004. *J. Climate,* **20,** 1713–1733.

——, S. W. Nesbitt, and L. D. Carey, 2009: On the correction of partial beam blockage in polarimetric radar data. *J. Atmos. Oceanic Technol.,* **26,** 943–957.

——, S. A. Rutledge, and R. Cifelli, 2010: Polarimetric radar observations of convection in northwestern Mexico during the North American Monsoon Experiment. *J. Hydrometeor.,* **11,** 1345–1357.

Lerach, D. G., S. A. Rutledge, C. R. Williams, and R. Cifelli, 2010: Vertical structure of convective systems during NAME 2004. *Mon. Wea. Rev.,* **138,** 1695–1714.

Liu, C., M. W. Moncrieff, and E. J. Zipser, 1997: Dynamical influence of microphysics in tropical squall lines: A numerical study. *Mon. Wea. Rev.,* **125,** 2193–2210.

Liu, H., and V. Chandrasekar, 2000: Classification of hydrometeors based on polarimetric radar measurements: Development of fuzzy logic and neuro-fuzzy systems, and in situ verification. *J. Atmos. Oceanic Technol.,* **17,** 140–164.

Lucas, C., and E. J. Zipser, 2000: Environmental variability during TOGA COARE. *J. Atmos. Sci.,* **57,** 2333–2350.

May, P. T., and T. D. Keenan, 2005: Evaluation of microphysical retrievals from polarimetric radar with wind profiler data. *J. Appl. Meteor.,* **44,** 827–838.

Medina, S., R. A. Houze Jr., A. Kumar, and D. Niyogi, 2010: Summer monsoon convection in the Himalayan region: Terrain and land cover effects. *Quart. J. Roy. Meteor. Soc.,* **136,** 593–616.

Mohr, C. G., L. J. Miller, R. L. Vaughan, and H. W. Frank, 1986: The merger of mesoscale datasets into a common Cartesian format for efficient and systematic analyses. *J. Atmos. Oceanic Technol.,* **3,** 143–161.

Nesbitt, S. W., R. Cifelli, and S. A. Rutledge, 2006: Storm morphology and rainfall characteristics of TRMM precipitation features. *Mon. Wea. Rev.,* **134,** 2702–2721.

——, D. J. Gochis, and T. J. Lang, 2008: The diurnal cycle of clouds and precipitation along the Sierra Madre Occidental observed during NAME-2004: Implications for warm season precipitation estimation in complex terrain. *J. Hydrometeor.,* **9,** 728–743.

Pereira, L. G., 2008: Characteristics and organization of precipitating features during NAME 2004 and their relationship to environmental conditions. Ph.D. dissertation, Atmospheric Science, Colorado State University, Fort Collins, CO, 229 pp.

Rickenbach, T. M., and S. A. Rutledge, 1998: Convection in TOGA COARE: Horizontal scale, morphology, and rainfall production. *J. Atmos. Sci.,* **55,** 2715–2729.

Romero, R., C. A. Doswell III, and R. Riosalido, 2001: Observations and fine-grid simulations of a convective outbreak in northeastern Spain: Importance of diurnal forcing and convective cold pools. *Mon. Wea. Rev.,* **129,** 2157–2182.

Rosenfeld, D., and C. W. Ulbrich, 2003: Cloud microphysical properties, processes, and rainfall estimation opportunities. *Radar and Atmospheric Sciences: A Collection of Essays in Honor of David Atlas, Meteor. Monogr.,* No. 52, Amer. Meteor. Soc., 237–237.

Rowe, A. K., S. A. Rutledge, T. J. Lang, P. E. Ciesielski, and S. M. Saleeby, 2008: Elevation-dependent trends in precipitation observed during NAME. *Mon. Wea. Rev.,* **136,** 4962–4979.

——, ——, and ——, 2011: Investigation of microphysical processes occurring in isolated convection during NAME. *Mon. Wea. Rev.,* **139,** 424–443.

Ryzhkov, A. V., T. J. Schuur, D. W. Burgess, P. L. Heinselman, S. E. Giangrande, and D. S. Zrnic, 2005: The Joint Polarization Experiment: Polarimetric rainfall measurements and hydrometeor classification. *Bull. Amer. Meteor. Soc.,* **86,** 809–824.

Srivastava, R. C., 1985: A simple model of evaporatively driven downdraft: Application to microburst downdraft. *J. Atmos. Sci.,* **42,** 1004–1023.

——, 1987: A model of intense downdrafts driven by the melting and evaporation of precipitation. *J. Atmos. Sci.,* **44,** 1752–1774.

Tessendorf, S. A., L. J. Miller, K. C. Wiens, and S. A. Rutledge, 2005: The 29 June 2000 supercell observed during STEPS. Part I: Kinematics and microphysics. *J. Atmos. Sci.,* **62,** 4127–4150.

Ulbrich, C. W., and D. Atlas, 2007: Microphysics of raindrop size spectra: Tropical continental and maritime storms. *J. Appl. Meteor. Climatol.,* **46,** 1777–1791.

van den Heever, S. C., and W. R. Cotton, 2004: The impact of hail size on simulated supercell storms. *J. Atmos. Sci.,* **61,** 1596–1609.

Williams, C. R., W. L. Ecklund, and K. S. Gage, 1995: Classification of precipitating clouds in the Tropics using 915-MHz wind profilers. *J. Atmos. Oceanic Technol.,* **12,** 996–1012.

Zrnić, D. S., and A. V. Ryzhkov, 1999: Polarimetry for weather surveillance radars. *Bull. Amer. Meteor. Soc.,* **80,** 389–406.